Protein Science (1999), *8*:2399–2405. Cambridge University Press. Printed in the USA.

X-ray crystallographic analysis of the structural basis for the interaction of pokeweed antiviral protein with guanine residues of ribosomal RNA

I.V. KURINOV,[1] F. RAJAMOHAN,[2] T.K. VENKATACHALAM,[3] AND F.M. UCKUN[4]

[1]Biotherapy Program, Department of Structural Biology, Hughes Institute, Roseville, Minnesota 55113
[2]Biotherapy Program, Department of Protein Engineering, Hughes Institute, Roseville, Minnesota 55113
[3]Biotherapy Program, Department of Chemistry, Hughes Institute, Roseville, Minnesota 55113
[4]Biotherapy Program, Department of Virology, Hughes Institute, Roseville, Minnesota 55113

(RECEIVED July 27, 1999; ACCEPTED August 31, 1999)

Abstract

Pokeweed antiviral protein (PAP) is a ribosome-inactivating protein (RIP), which enzymatically removes a single adenine base from a conserved, surface exposed loop sequence of ribosomal rRNA. We now present unprecedented experimental evidence that PAP can release not only adenine but guanine as well from *Escherichia coli* rRNA, albeit at a rate 20 times slower than for adenine. We also report X-ray structure analysis and supporting modeling studies for the interactions of PAP with guanine. Our modeling studies indicated that PAP can accommodate a guanine base in the active site pocket without large conformational changes. This prediction was experimentally confirmed, since a guanine base was visible in the active site pocket of the crystal structure of the PAP-guanine complex.

Keywords: active site interactions; guanine release; ribosome inactivating proteins; X-ray crystallography

Pokeweed antiviral protein (PAP) from the leaves of the pokeweed plant, *Phytolacca americana*, is a naturally occurring 29 kDa single chain ribosome inactivating protein (RIP), which catalytically inactivates both prokaryotic and eukaryotic ribosomes. The therapeutic potential of PAP has gained considerable interest in recent years due to the clinical use of native PAP as the active moiety of immunoconjugates against cancer and AIDS (Irvin & Uckun, 1992).

PAP is a site-specific RNA N-glycosidase that enzymatically removes a single adenine base (A4324) from a highly conserved, surface exposed "α-sarcin" loop with the GAGAG motif (the cleaved adenine is underlined) of the large rRNA species in eukaryotic (28S rRNA) and prokaryotic (23S rRNA) ribosomes (Irvin, 1983; Endo et al., 1988). This catalytic depurination of the α-sarcin loop, which is positioned in immediate vicinity of the peptidyl-transferase center within the 50 S subunit of *Escherichia coli* ribosomes, impairs the interactions between ribosomes and elongation factor 2 (EF-2), resulting in irreversible inhibition of protein synthesis at the EF-2 mediated translocation step (Gessner & Irvin, 1980).

PAP has also been shown to effectively inhibit the replication of several plant and animal viruses including poliovirus, herpes simplex virus, cytomegalovirus, influenza virus, and human immunodeficiency virus (HIV)-1 (Zarling et al., 1990; Irvin & Uckun, 1992). The molecular mechanism of the antiviral activity of PAP is under active investigation (Bonness et al., 1994; Chaddock et al., 1996; Xu et al., 1998). Besides its ability to inhibit viral protein synthesis, PAP is also capable of directly depurinating viral RNA (Barbieri et al., 1997; Rajamohan et al., 1999). Furthermore, PAP also displays viral RNA-specific effects in vivo and has been shown to inhibit ribosomal frameshifting and retrotransposition, a molecular mechanism used by many RNA viruses to produce Gag-Pol fusion proteins (Tumer et al., 1998).

Wild-type PAP was crystallized and its structure was refined both at room temperature (Monzingo et al., 1993) and lower temperatures (Kurinov et al., 1999). To date, no structural information has been reported regarding the interaction of PAP with its natural substrates. A working hypothesis regarding the structural basis for the N-glycosidase activity of PAP was proposed based on the structural similarities of the active sites of PAP and ricin A-chain, a more extensively analyzed RIP (Monzingo & Robertus, 1992).

Here, we present unprecedented experimental evidence that PAP can release not only adenine but guanine as well from rRNA. We also report X-ray structure analysis and supporting modeling studies of the interactions of PAP with guanine. In particular, guanine was cocrystallized with PAP, and computer modeling studies were performed to elucidate the structural basis of its interactions with PAP. Our modeling studies indicated that PAP can accommodate a guanine base in the active site pocket without large conformational changes. This prediction was experimentally confirmed, since a guanine base was visible in the active site pocket of the crystal structure of the PAP-guanine complex. GMP can be also fit into the PAP active site pocket without any distortion of the active site geometry, forming a weak complex with PAP.

Reprint requests to: I.V. Kurinov, Hughes Institute, 2665 Long Lake Road, Roseville, Minnesota 55113; e-mail: igor@ih.org.

Results and discussion

Depurination of E. coli rRNA by PAP

We examined PAP for depurinating activity against *E. coli* rRNA using both adenine release assays and guanine release assays. The amounts of adenine and guanine released from the substrate rRNA were measured using quantitative high-performance liquid chromatography (HPLC), as described in Materials and methods. Under the described chromatographic conditions, the retention time for adenine was 9.2 min (Rajamohan et al., 1999). By comparison, the retention time for guanine was 4.9 min. At this retention time, guanine was eluted without an interference peak from the blank control (Fig. 1). The calibration curve for guanine was linear between 5 to 125 pmol and could be described by the regression equation: $Y = 2.074X + 1.193$ ($r \sim 0.999$), where Y is the amount of guanine recovered in pmol and X is the absolute peak area. The lowest limit of detection of guanine was 3.0 pmol at a signal to noise ratio of ≈3. The intra- and interassay coefficients of variation were less than 5% for both the adenine- and guanine-release assays. The overall intra- and interassay accuracies of this method were 98.7 ± 1.7% ($N = 3$) and 95.7 ± 3.3% ($N = 3$), respectively, for the adenine release assays, and 100.9 ± 2.8% ($N = 3$) and 100.5 ± 4.2% ($N = 3$), respectively, for the guanine release assays. Using the linear portions of the concentration-dependent depurination curves (Fig. 2), we estimated that at a concentration of 5 μM (4 h incubation), PAP released 154 ± 10 pmol of adenine and 7.6 ± 1.5 pmol of guanine, respectively, from 1 μg of *E. coli* rRNA. Thus, PAP can both deadenylate and deguanylate rRNA, but it is 20-fold more efficient in deadenylation.

Crystallographic studies of PAP interactions with guanine

Our data had revealed a noticeable amount of free guanine released during *E. coli* rRNA depurination by PAP. To better understand the interaction of PAP with guanine-containing oligonucleotides, we cocrystallized PAP with guanine. Crystals of the PAP-guanine complex have the same space group and very similar unit cell parameters as the crystal of ligand-free PAP. The initial $2F_o - F_c$ electron density map for PAP complexed with guanine showed continuous electron density in the active site pocket. This density was initially fitted with guanine having the same overall orientation as the adenine base from our previous X-ray studies of PAP-adenine complexes (Kurinov et al., 1999). After the crystallographic refinement the omit electron density maps showed bulky electron density covering the guanine base (Fig. 3). The precision of the electron density map was not sufficient to accurately position the guanine base in the active site. Therefore, we used a computer modeling to identify an energetically favorable position for guanine. Our modeling simulation showed that guanine should be more tightly bound in the conformation having the ~180° flip from the original adenine-like binding mode. Figure 4 illustrates the binding interactions of guanine with the active site residues of PAP. Orientation of the Tyr72 in the PAP-guanine complex remains the same as in the ligand free-form of PAP. The guanine ring is sandwiched between Tyr72 and Tyr123 (Fig. 4). N7 of guanine receives a hydrogen bond from the amino nitrogen of Val73 (distance 3.3 Å). The amino group of Arg179 can donate two hydrogen bonds to O6 (distance 2.8 Å) and N9 is hydrogen bonded to the carbonyl oxygen of Ser121 (2.8 Å). It is worth noting that this conformation of the guanine base is prohibited for the GMP binding mode because of severe collision of the attached sugar moiety with the PAP protein. The only noticeable difference between this complex and the more strongly bound complex of PAP with adenine is the overall orientation of the purine base. A weaker interaction of guanine with PAP is also illustrated by the featureless electron density covering guanine.

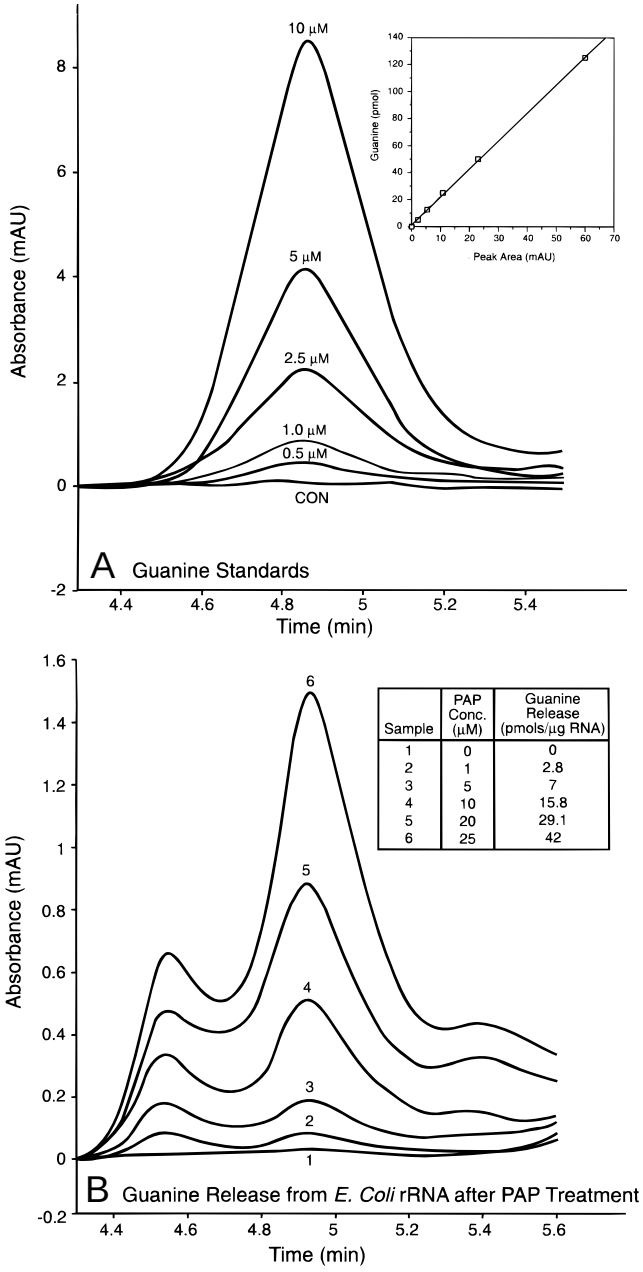

Fig. 1. HPLC-based detection of guanine released from *E. coli* rRNA. **A:** Chromatogram of guanine standard showing peak area and response time. **Inset**: Standard curve of guanine standards. **B:** Representative chromatogram of guanine release from *E. coli* 16S- and 23S-rRNA after treatment with increasing concentrations of PAP. Experimental conditions are described in Materials and methods.

Our previous modeling studies of PAP had indicated that the adenine interactions with the active site and the phosphate backbone are the main contributors to the strong binding of GAGAG fragment

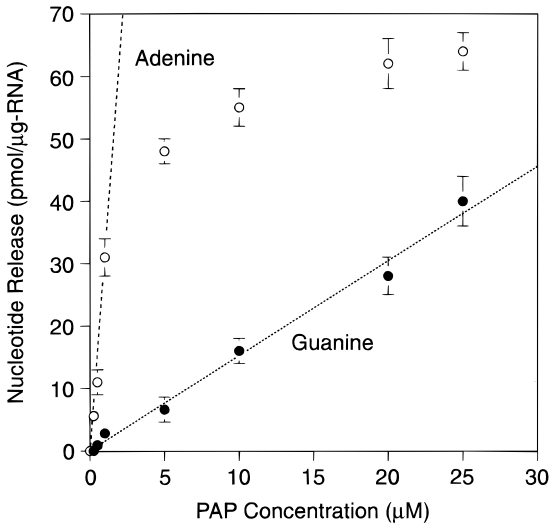

Fig. 2. Concentration-dependent release of adenine and guanine from *E. coli* rRNA after PAP treatment. Values were calculated using the standard curves for adenine and guanine. Lines were constructed by linear regression using the data points from the exponential phase. The experimental conditions are as described in Materials and methods.

by PAP. We predicted that the adenine specificity of PAP is determined only by the active site, which strongly binds the adenine base. Two neighboring guanines close to the bound adenine do not have any strong and specific interactions with PAP. The broad reactivity of PAP toward rRNA from different sources can be explained by a limited specificity of PAP toward adenine. Our experimental results demonstrate that PAP has a high affinity toward purines-containing oligonucleotides without a high degree of selectivity toward the closest nucleotide residues in the RNA/DNA sequence.

To determine if a guanosine molecule can fit into PAP active site, we also performed a molecular docking of GMP to PAP. Our modeling studies showed that GMP can be complexed with PAP without disturbing the unique geometry of the active site (Fig. 5). The best overall orientation of the GMP guanine base in the active site is similar to that has been observed experimentally for nucleotide analogs (Monzingo et al., 1993) and adenine (Kurinov et al., 1999). Although this mode of GMP binding to PAP is not very strong, this conformation may be favorable for enzymatic cleavage of the C-N bond. Indeed two PAP residues, which are believed to be responsible for the adenine cleavage (Arg179 and Gln176) (Monzingo et al., 1993), are rather close to the cleavable bond in the PAP-GMP complex and probably can participate in the enzymatic cleavage of guanine from ribosomal RNA upon a small structural rearrangement due to the overall protein flexibility.

Materials and methods

Adenine and guanine release assays

Adenine and guanine were purchased from Sigma Chemicals (St. Louis, Missouri). *E. coli* rRNA (16S- and 23S-ribosomal RNA) was purchased from Boehringer Mannheim (Indianapolis, Indiana). The HPLC-based guanine detection system consisted of a

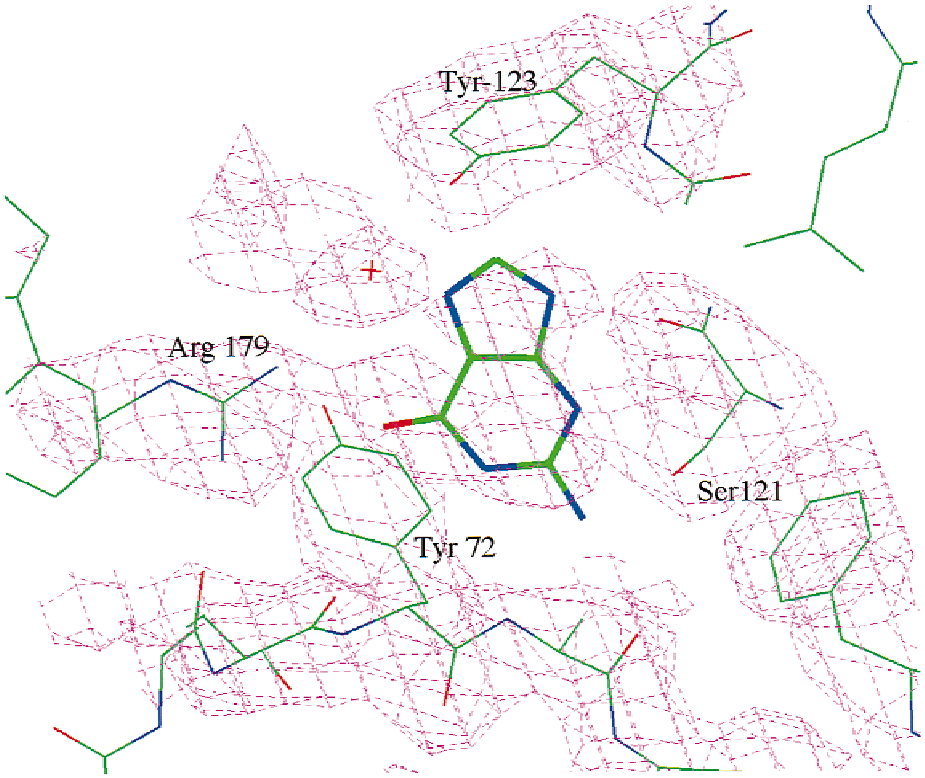

Fig. 3. Omit electron density map ($F_o - F_c$) for PAP-guanine complex at room temperature. Guanine and protein residues within 4 Å were omitted for map calculations. Model for guanine is drawn in bold. The map is contoured at 1.5σ.

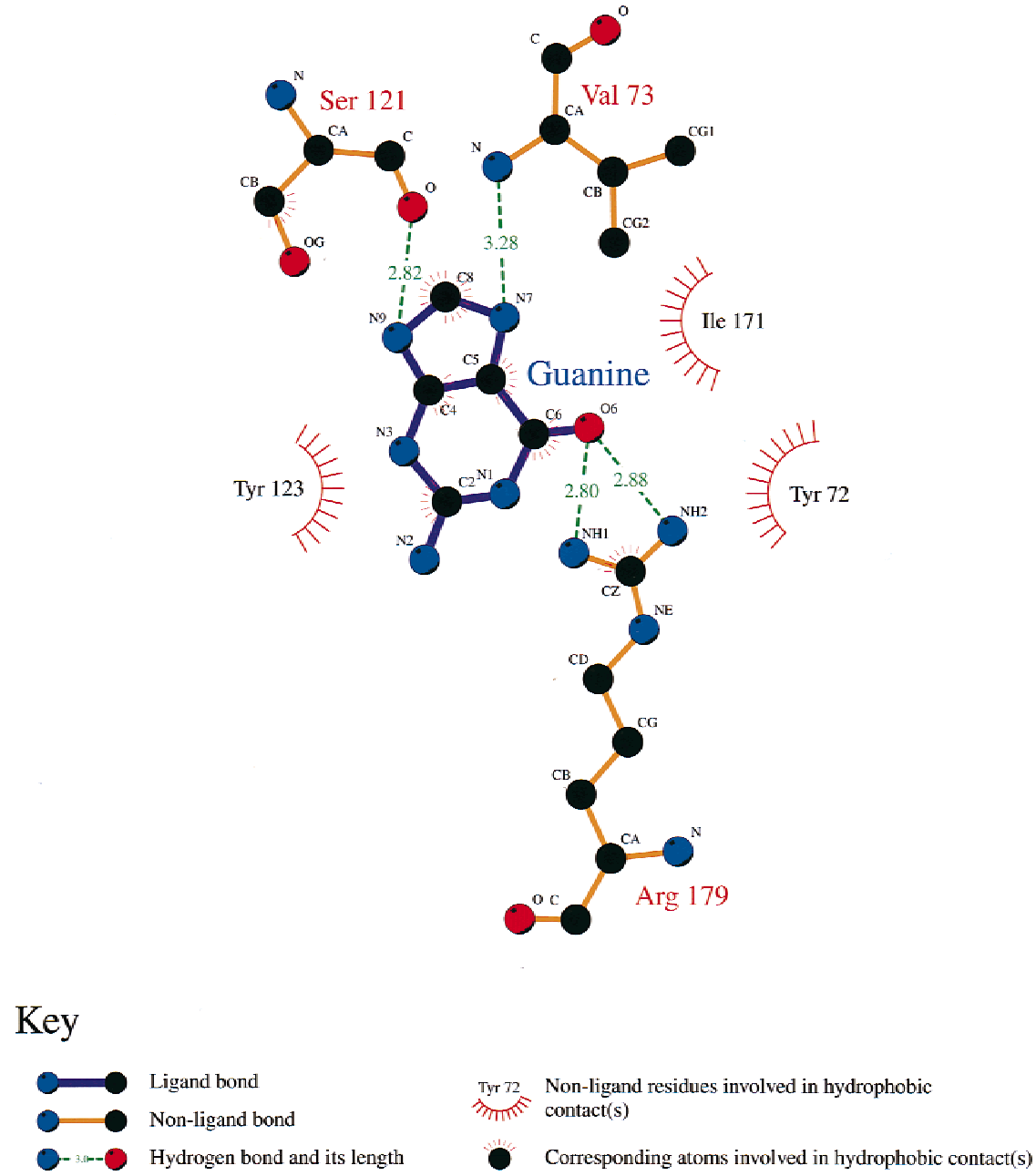

Fig. 4. Details of interaction of guanine with active site residues of PAP. The figure was drawn using LIGPLOT (Wallace et al., 1995).

Hewlett Packard (HP) series 1100 (Hewlett Packard, Palo Alto, California) in conjunction with a quaternary pump, an autosampler, an auto electronic degasser, an automatic thermostatic column compartment, diode array detector, and a computer with a Chemstation software program for data analysis. Release of adenine and guanine from RNA substrates was determined using a reverse-phase Lichrospher 100, RP-18 analytical column (Hewlett-Packard, 5 mm particle size, 250 × 4 mm). The HPLC running buffer (50 mM $NH_4C_2H_3O_2$, 5% methanol, pH 5.0) was used as the mobile phase. The column was equilibrated and eluted under isocratic conditions at a flow rate of 1.0 mL/min.

E. coli rRNA samples (2 μg) were incubated with increasing concentrations (0.25, 0.5, 1.0, 5.0, 10, 20, and 25 μM) of PAP for 4 h at 37 °C in 50 μL of binding buffer (25 mM Tris HCl, pH 7.8, 10 mM KCl, 5 mM $MgCl_2$, 2% glycerol). The reaction was stopped by adding 100 μL of HPLC running buffer and 100 μL of the sample was injected automatically into the Lichrospher 100RP-18E column. The detector wavelength was set at 260 nm, and the flow rate was maintained at 1 mL/min. Controls included samples containing (1) PBS-treated *E. coli* rRNA and (2) PAP without rRNA.

Calibration curve

A calibration curve was generated to confirm the linear relationship between the absolute peak area and the quantities of adenine

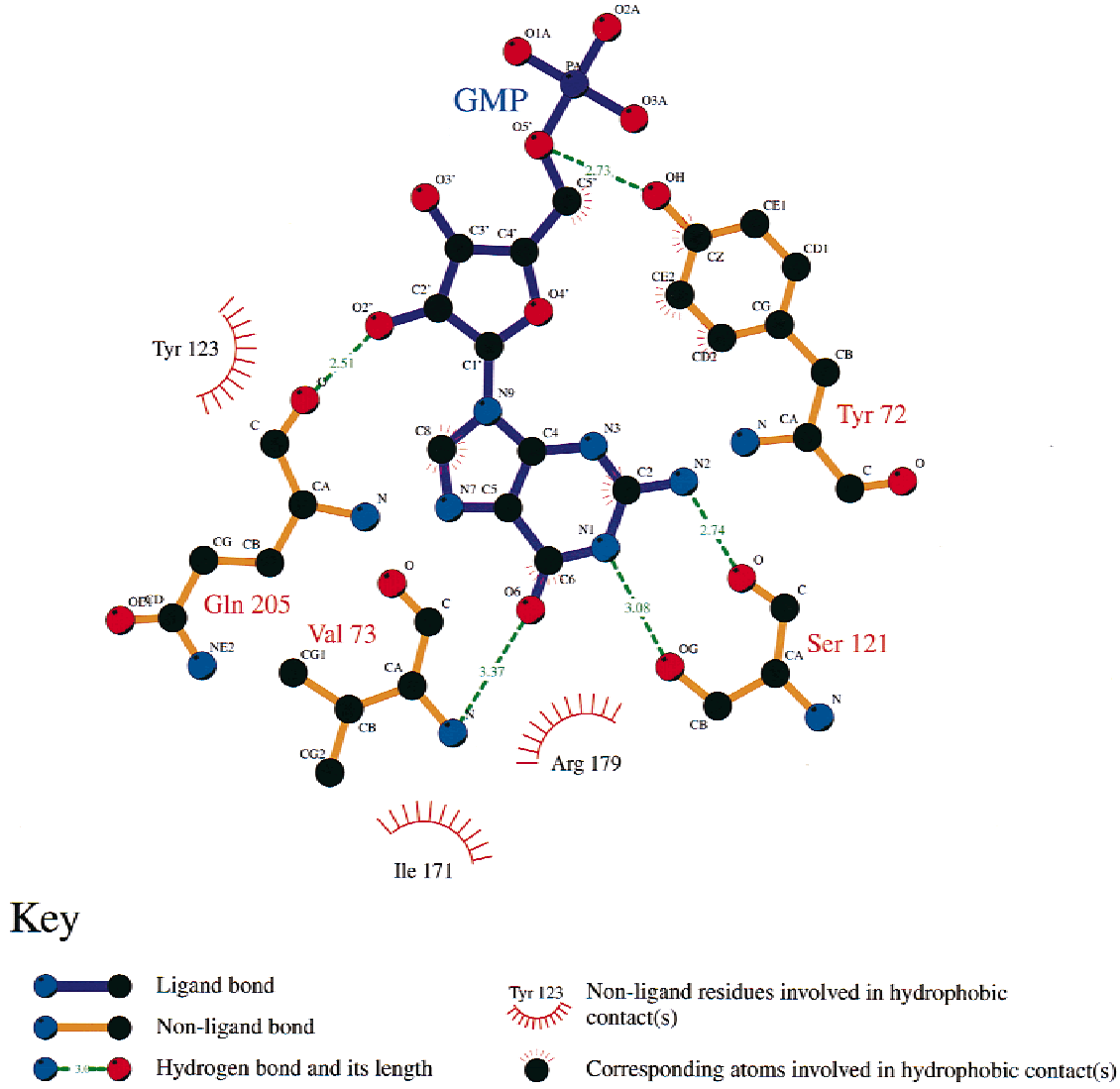

Fig. 5. Details of interaction of GMP with active site residues of PAP. The figure was drawn using LIGPLOT (Wallace et al., 1995).

or guanine in the tested samples. Adenine and guanine at final concentrations of 0.1 μM (= 5 pmol/50 μL), 0.25 μM (= 12.5 pmol/50 μL), 0.5 μM (= 25 pmol/50 μL), 1.0 μM (= 50 pmol/50 μL), 2.5 μM (= 125 pmol/50 μL) were injected into the HPLC system for analysis, and the calibration curves were generated by plotting the absolute peak area against the quantities of adenine or guanine. Unweighted linear regression analysis of the calibration curve was performed by using the CA-Cricket Graph III computer program, version 1.1 (Computer Association, Inc., Islandia, New York).

Intraassay and interassay accuracy and precision

To evaluate the intra-assay accuracy and precision, standard samples containing 0.5 or 2.5 μM adenine or guanine were prepared and analyzed within a single day, and the quantities were calculated using the calibration curve as described above. The ratio of the calculated quantities over the known quantities spiked was calculated to evaluate the intra-assay precision. The interassay accuracy was calculated as the ratio of the calculated quantities over the known quantities using data from three independent experiments. The interassay precision was estimated by determining the coefficient of variation from three independent experiments.

Protein purification and crystallization

PAP was extracted from spring leaves of pokeweed and purified to homogeneity as previously described (Myers et al., 1991). Immediately prior to the crystallization setup, PAP was repurified on a MonoS cation-exchange column (Pharmacia Biotech, Piscataway, New Jersey) and filtered through a 0.22 μm filter. Guanine was purchased from Sigma (St. Louis, Missouri).

PAP crystals were obtained from a concentrated PAP preparation (15–20 mg/mL) by the vapor diffusion method within 1 week using "hanging drop" experiments with 22% PEG 4000 and 0.1 M $CaCl_2$ (50 mM Tris-HCl buffer pH = 8) at room temperature with the addition of 5 mM guanine. Unit cell parameters, details of data collection and refinement are presented in Table 1. Diffraction data

Table 1. *Details of data collection and refinement for PAP-guanine complex*

	PAP-guanine complex
Unit cell (Å)	
(*a*)	49.29
(*b*)	49.41
(*c*)	64.29
a	68.66
b	81.04
g	63.87
R-merge (%)	6.7
Resolution limit for refinement	2.1
Completeness of data used for refinement (%)	87.0
R-factor (%)	19.2
Number of water molecules	552
Protein *B*-factor (A^2)	24.6
Guanine *B*-factor (A^2)	44.0

were collected on a Rigaku RaxisIY imaging plate. The X-ray source was a copper Rigaku RU300H generator with a double mirror system operating at 50 kV and 100 mA. The crystal-to-detector distance was 150 mm, and the crystal in two different orientations was rotated around the spindle axis with images collected over 1.5° to a resolution of 2.1 Å. Data were evaluated using the HKL package (DENZO and SCALEPACK; Otwinowski & Minor, 1998). The completeness of data sets was over 87% when the completeness of the data set in the last resolution shell was over 80%.

Model refinement

The atomic coordinates of our refined ligand-free PAP structure (PDB access code 1QCG) were used for the initial crystallographic phasing and refinement of the new PAP complex. All calculations were done using X-PLOR (version 3.1) (Brünger, 1992). All data with $I/\sigma > 2$ and a low-resolution limit of 8 Å were used for structure refinement. Nonpolar hydrogens were implicitly included in their associated heavy atoms. There were two PAP monomers per unit cell, and they are approximately related by a twofold symmetry nearly coincident with the crystallographic α-axis. At the early stage of the crystallographic refinement, strong noncrystallographic symmetry (NCS) restraints were imposed to keep the structure of two PAP molecules close and not to increase the free *R*-factor. As the refinement progressed, the values of the effective energy constant for the positional restraints between two monomers were relaxed from 300 to 60 kcal/mol/$Å^2$ for the main-chain atoms and 30 kcal/mol/$Å^2$ for the side-chain atoms. Complete removal of NCS restrains led to a small increase of *R*-free factor.

There are no large conformational differences between the two PAP molecules of the asymmetric unit because of noncrystallographic symmetry restraints imposed during the crystallographic structure refinement. The root-mean-square deviation (RMSD) was 0.05 Å for the main chain and 0.13 Å for side-chain atoms between two PAP monomers. Overall conformation and mode of interaction of guanine were the same in two monomers. For the subsequent structural comparison, the average values of the two models were used.

A few cycles of slow-cooling annealing (3,500 → 100 K), positional and restrained isotropic temperature factor refinements were followed by visual inspection of electron density maps, including omit maps, coupled with a manual model building (when necessary) using the graphics program CHAIN (Sack, 1988). All atom occupancies were set to one and were not refined. Strong stereochemical restraints were imposed during the crystallographic refinement and final PAP structure possessed a good stereochemistry with RMSD of ~0.006 Å for bond lengths and ~1.25° for angles. The quality of the stereochemistry of the final protein structure was assessed with the PROCHECK package (Laskowski et al., 1993). The Ramachandran plot did not reveal any residues in disallowed regions (data not shown). As a better guide to the quality of the structure, the values of the free *R*-factor were monitored during the course of the crystallographic refinement. The final value of free *R*-factors did not exceed the overall *R*-factor by more than 8%.

The refined coordinates of PAP complex with guanine have been deposited in Protein Data Bank (PDB) (ID code 1DGA).

Ligand docking modeling

The molecular docking of ligands and estimation of the interaction scores were done using a Fixed Docking procedure in the Affinity program within the InsightII modeling software (MSI, 1996). The initial position of the guanine base was manually docked based on the position of the adenine base in the PAP active site (PDB access code 1QCI) (Kurinov et al., 1999). The second starting position had a 180° flip without any steric collision with protein. These two general positions of guanine were used for subsequent docking trials. Because of the sterical collisions, the guanine base of GMP could be positioned only in one conformation, similar to the adenine base position in the PAP-adenine complex. To increase the volume of the conformational search, the torsion angles in GMP molecules between N9 of guanine and phosphate group were freed. We created a definitive binding set of PAP residues in the active site pocket to move as a 3.5 Å shell around the manually docked ligand during the energy minimization. The number of final docking positions was set to 10, although finally only 2–4 promising positions were identified. The calculations used a CVFF forcefield in the Discovery program and a Monte Carlo strategy in the Affinity program. Each energy-minimized final docking position of the ligand was evaluated using the interactive score function in the Ludi module. Ludi score includes contribution of the loss of translational and rotational entropy of the fragment, number and quality of hydrogen bonds, and contributions from ionic and lipophilic interactions to the binding energy.

Acknowledgments

The authors thank K. Chang for his technical assistance. This material is based in part upon work sponsored by the Defense Advanced Research Projects Agency under Grant N65236-99-1-5422 awarded to F.M.U. The content does not necessarily reflect the position or policy of the U.S. Government, and no official endorsement should be inferred.

References

Barbieri L, Valbonesi P, Bonora E, Gorini P, Bolognesi A, Stirpe F. 1997. Polynucleotide: Adenosine glycosidase activity of ribosome-inactivating proteins:effect on DNA, RNA, and poly(A). *Nucleic Acids Res 25*:518–522.

Bonness MS, Ready MP, Irvin JD, Mabry TJ. 1994. Pokeweed antiviral protein inactivates pokeweed ribosomes: Implications for the antiviral mechanism. *Plant J 5*(2):173–183.

Brünger AT. 1992. *X-PLOR (version 3.1) manual*. New Haven: Yale University Press. 405 pp.

Chaddock JA, Monzingo AF, Robertus JD, Lord JM, Roberts LM. 1996. Major structural differences between pokeweed antiviral protein and ricin A-chain do not account for their differing ribosome specificity. *Eur J Biochem 235*(1–2):159–166.

Endo Y, Tsurugi K, Lambert JM. 1988. The site of action of six different ribosome-inactivating proteins from plants on eukaryotic ribosomes: The RNA N-glycosidase activity of the proteins. *Biochem Biophys Res Commun 150*(3):1032–1036.

Gessner SL, Irvin JD. 1980. Inhibition of elongation factor 2-dependent translocation by the pokeweed antiviral protein and ricin. *J Biol Chem 255*:3251–3253.

Irvin JD. 1983. Pokeweed antiviral protein. *Pharmacol Ther 21*:371–387.

Irvin JD, Uckun FM. 1992. Pokeweed antiviral protein: Ribosome inactivation and therapeutic applications. *Pharmacol Ther 55*(3):279–302.

Kurinov IV, Myers DE, Irvin JD, Uckun FM. 1999. X-ray crystallographic analysis of the structural basis for the interactions of pokeweed antiviral protein with its active site inhibitor and ribosomal RNA substrate analogs. *Protein Sci 8*:1765–1772.

Laskowski RA, MacArthur MW, Moss DS, Thornton JM. 1993. PROCHECK: A program to check the stereochemical quality of protein structures. *J Appl Crystallogr 26*:283–291.

Monzingo AF, Collins EJ, Ernst SR, Irvin JD, Robertus JD. 1993. The 2.5 Å structure of pokeweed antiviral protein. *J Mol Biol 233*(4):705–715.

Monzingo AF, Robertus JD. 1992. X-ray analysis of substrate analogs in the ricin A-chain active site. *J Mol Biol 227*(4):1136–1145.

MSI. 1996. *InsightII user guide*. San Diego, California: MSI/Biosym.

Myers DE, Irvin JD, Smith RS, Kuebelbeck VM, Uckun FM. 1991. Production of a pokeweed antiviral protein (PAP)-containing immunotoxin, B43-PAP, directed against the CD19 human B lineage lymphoid differentiation antigen in highly purified form for human clinical trials. *J Immunol Methods 136*:221–237.

Otwinowski Z, Minor W. 1998. Processing of X-ray diffraction data collected in oscillation mode. *Methods Enzymol 276*:307–325.

Rajamohan F, Venkatachalam TK, Irvin JD, Uckun FM. 1999. Pokeweed antiviral protein isoforms PAP-I, PAP-II, and PAP-III depurinate RNA of human immunodeficiency virus (HIV)-1. *Biophys Biochem Research Comm 260*: 453–458.

Sack JS. 1988. CHAIN: A crystallographic modeling program. *J Mol Graph 6*:224–225.

Tumer NE, Parikh BA, Li P, Dinman JD. 1998. The pokeweed antiviral protein specifically inhibits Ty1-directed +1 ribosomal frameshifting and retrotransposition in Saccharomyces cerevisiae *J Virol 72*(2):1036–1042.

Wallace AC, Laskowski RA, Thornton JM. 1995. LIGPLOT: A program to generate schematic diagrams of protein-ligand interactions. *Protein Eng 8*(2):127–134.

Xu J, Meng AX, Hefferon KL, Ivanov IG, Abouhaidar MG. 1998. Effect of N-terminal deletions on the activity of pokeweed antiviral protein expressed in *E. coli*. *Biochimie 80*(12):1069–1076.

Zarling JM, Moran PA, Haffar O, Sias J, Richman DD, Spina CA, Myers DE, Kuebelbeck V, Ledbetter JA, Uckun FM. 1990. Inhibition of HIV replication by pokeweed antiviral protein targeted to CD4+ cells by monoclonal antibodies. *Nature 347*(6288):92–95.